

## CHARACTERIZATION OF SbSI NANOCRYSTALS BY ELECTRON MICROSCOPY, X-RAY DIFFRACTION AND RAMAN SCATTERING

I. M. Voynarovych, A. V. Gomonnai<sup>a</sup>, A. M. Solomon<sup>a</sup>, Yu. M. Azhniuk<sup>a</sup>, A. A. Kikineshi<sup>\*</sup>, V. P. Pinzenik, M. Kis-Varga<sup>b</sup>, L. Daroczy<sup>c</sup>, V. V. Lopushansky<sup>a</sup>

Uzhhorod National University, Pidhirna St. 46, Uzhhorod, 88000, Ukraine

<sup>a</sup>Institute of Electron Physics, Ukr. Nat. Acad. Sci., Universytetska St. 21, Uzhhorod, 88017, Ukraine

<sup>b</sup>Institute of Nuclear Research, Hungar. Acad. Sci., P.O.Box 51, 4001, Debrecen, Hungary

<sup>c</sup>Department of Solid State Physics, University of Debrecen, P.O. Box 2, 4010, Debrecen, Hungary

X-ray diffraction and electron microscopy data show the crystal lattice structure and rod-like shape of SbSI nanocrystals obtained by ball milling to be similar to that of the bulk crystals. The dependence of the grain size on the milling duration is considered in view of the chain-like crystalline structure of SbSI. The observed Raman line broadening is discussed in the frame of confinement-related selection rules relaxation and scattering by surface phonons.

(Received July 11, 2003; accepted July 31, 2003)

*Keywords:* Nanocrystals, Raman spectroscopy, X-ray diffraction, Transmission electron microscopy

### 1. Introduction

The studies of nanoscale ferroelectrics have shown that their parameters can strongly depend on the crystallite size [1–4]. For this reason it seemed interesting in view of both fundamental and applied physical aspects to obtain and investigate nanocrystals of antimony sulphoiodide, since so far there has been only a single recent publication on nanometric SbSI, obtained by sol-gel method [5] and a paper on the effect of thermal annealing on the structural properties of the SbSi glass [6].

Here we report the results on obtaining SbSI nanocrystals by mechanical milling and their characterization by transmission electron microscopy, X-ray diffraction and Raman scattering which proved to be well elaborated techniques for characterization of size, shape and structure of mesoscopic and nanoscale materials.

### 2. Experimental

The single crystals of SbSI were grown by chemical transport, the relevant growth details being described in [7]. Ball milling in a cylindrical vial of stainless steel with a hardened steel ball, similar to that described in [8], was applied to obtain microcrystalline powders of various grain size. The vial and the ball were kept in motion by a vibrating frame (type Fritsch Pulverisette 0). Prior to milling the vial was evacuated and sealed. The 50-h milling process was interrupted after 1-, 2-, 3-, 4- 5- and 25-h periods and each time a small amount of powder was taken for investigation. The grain size reduction achieved during each milling step was followed by measuring X-ray diffraction spectra of powders with a horizontal Siemens diffractometer by using Cu  $K_{\alpha 1}$  radiation.

<sup>\*</sup>Corresponding author: kiki@tigris.klte.hu

For transmission electron microscopy (TEM) investigations the ball-milled powder was mixed with epoxy resin and a thin layer of this mixture was spread between two silicon wafers. This structure was embedded into a 3-mm-diameter aluminium disc. After the epoxy being cured the sample was ground and polished mechanically from both sides. The final thinning was performed with low-angle ( $<5^\circ$ ) Ar-ion treatment. A JEOL 2000 FX-II transmission electron microscope equipped with an Oxford Link-Isis EDS system was used for the TEM measurements.

Raman scattering measurements were performed at room temperature on a LOMO DFS-24 double grating monochromator with a FEU-79 phototube and a photon counting system, the excitation being provided by a He–Ne laser (632.8 nm). The instrumental width did not exceed  $1 \text{ cm}^{-1}$ .

### 3. Results and discussion

The X-ray diffraction (XRD) analysis (Fig. 1) has confirmed that SbSI lattice structure is preserved for the nanocrystalline samples, though the diffraction peaks become broader and less pronounced with the size decrease. Moreover, XRD data can be applied to estimate the crystallite average size from the halfwidth of reflection profiles. For spherical or near-spherical crystallites the grain size can be calculated from the known Scherrer equation [9]

$$d = \frac{\lambda}{\Delta(2\theta)\cos\theta_0} \quad (1)$$

where  $d$  is the average nanocrystal diameter,  $\lambda$  is the X-ray wavelength,  $\Delta(2\theta)$  is the diffraction peak halfwidth,  $\theta_0$  is the diffraction angle.

However, for needle-shaped crystallites such method can hardly be applicable since the notion "average size" cannot be clearly specified. In this case the method of Fourier harmonic analysis of the diffraction patterns [10] can be applied, in order to evaluate the average crystallite dimensions in different crystallographic directions.

If  $H$  and  $G$  are the Fourier images of the diffraction peak in the nanometric powder and the reference microcrystal, then the dependence of the value

$$A = (H_{\text{Re}} G_{\text{Re}} + H_{\text{Im}} G_{\text{Im}}) / (G_{\text{Re}}^2 + G_{\text{Im}}^2) \quad (2)$$

(indices Re and Im denoting the real and imaginary part, respectively) on the running number  $n$  of the atomic plane in the column of the reflecting atomic planes can be built, where  $n = (2t \tan \theta_0 / l \alpha) t$ ,  $l$  is the number of the reflection order,  $\alpha$  is the angular range of the observed peak, used for Fourier imaging,  $t$  is a running number [10].

The Fourier data processing has shown that nanocrystals are formed mostly during the first hour of milling, while the subsequent two hours reduce the average transverse size  $d$  by  $\sim 12\%$ , and the rest of the 50-h milling process results in another  $\sim 13\%$  decrease of  $d$ .

As seen from the TEM studies (an image of one of the fractions of the obtained SbSI microcrystalline powders is shown in Fig. 2), the obtained crystallites are of needle-like shape similar to that of bulk SbSI crystals and quite different from the generally spherical shape of SbSI nanocrystals obtained in [5] by sol-gel method. The formation of the rod-shaped crystallites under milling can be, in our opinion, related to the chain-like crystalline structure of SbSI where four formula units in the unit cell form the elements of two chains with the intrachain forces of ionic and covalent nature and weak van der Waals interchain forces [11].

Mechanical fracture of crystalline materials begins from their breaking down at the defects with minimal strength (macro- and microcracks). Hence, in the course of attrition the strength of the crystallites increases what results in a considerable increase of energy being dissipated for further milling. It is quite reasonable to suppose that the smaller and less deficient crystals will break down more probably in the directions where the van der Waals forces act. That is why the shape of the milled crystallites resembles that of the bulk samples.

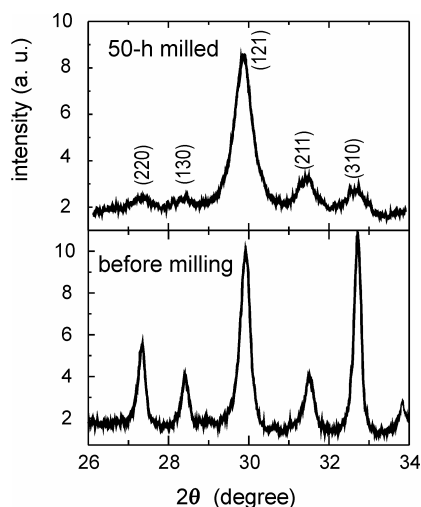


Fig. 1. X-ray diffraction patterns for SbSI micro- and nanocrystals.

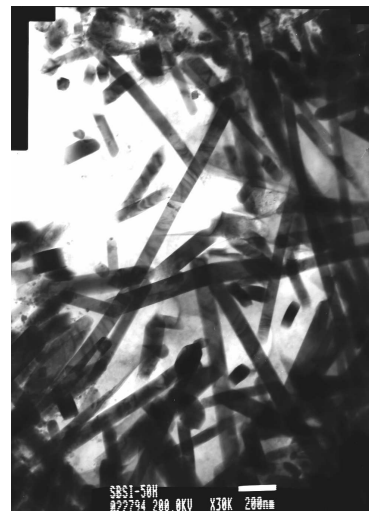


Fig. 2. TEM image of SbSI powder after 50-h milling.

As can be estimated from the TEM image of Fig. 2, the length of the rod-shaped SbSI crystallites after 50-h milling varied from 0.5 to 1  $\mu\text{m}$  while their thickness was mostly within 50–100 nm. The histogram, shown in Fig. 3, enabled us to estimate the average rod thickness of about 70 nm and its dispersion. It should be noted that thus directly determined size parameter is somewhat higher than that estimated from XRD, since in fact the true diffraction broadening results from the contributions of two factors – the crystallite size and microstrain, the latter arising from the weak interchain van der Waals forces. Thus, the observed rapid decrease of the average thickness of the rods in the first hour of milling down to 80–100 nm and its subsequent slowdown are quite consistent with the above discussed increase of the nanocrystal hardness in the course of milling.

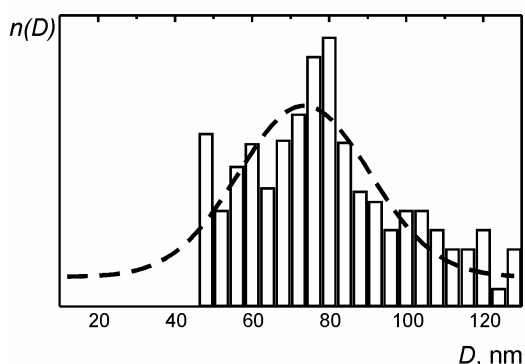


Fig. 3. Histogram of SbSI nanocrystal thickness distribution after 50 h milling.

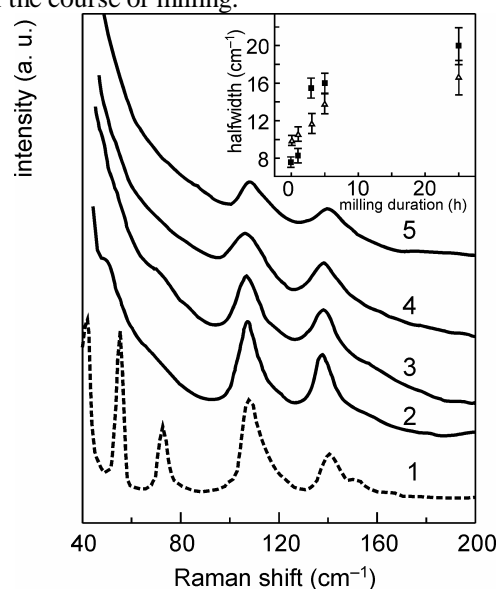


Fig. 4. Raman spectra of SbSI crystallites before milling (2) and after 1-h (3), 3-h (4) and 25-h (5) milling compared with the bulk crystal spectrum, taken from [12] (1). The insert shows the Raman halfwidth dependence for SbSI crystallites on the milling duration for the bands centred at 107  $\text{cm}^{-1}$  (open triangles) and 139  $\text{cm}^{-1}$  (solid squares).

Fig. 4 illustrates the measured Raman spectra of nanocrystalline SbSI powder fractions, obtained by milling of different duration, which are compared with the bulk crystal spectrum from Ref. 12. In the low-frequency range (below  $100 \text{ cm}^{-1}$ ), where for the bulk crystal a rich phonon spectrum is reported [12–14] (curve 1), in the spectra of powder samples the phonon bands are seen to be smeared, masked in the Rayleigh scattering wing, the intensity of the latter increasing with the size reduction. Only for microcrystalline powders (curve 2) and the first nanometric powder fraction (curve 3) some features in the low-frequency range can be detected. Meanwhile the Raman bands at  $107$  and  $139 \text{ cm}^{-1}$  are clearly observed for all nanometric samples. It should be noted that the frequencies of the discussed two bands are practically independent of the milling duration, i.e. of the nanocrystal size, while their halfwidths appear to grow continuously in the course of the milling, the relevant dependence being plotted in the insert of Fig. 4.

Such kind of behaviour of Raman band parameters on the crystallite size is rather typical for semiconductor microcrystals whose Raman spectra were thoroughly studied e. g. for Si [15,16,17], GaP [15],  $\text{CdS}_{1-x}\text{Se}_x$  [18–20]. It should be noted that, contrary to our case, the size decrease-induced broadening is, as a rule, accompanied by slight downward shift of the peak frequencies and Raman band asymmetry with a more pronounced low-frequency wing. Generally the observed features are most often explained by confinement-related selection rules relaxation due to the small crystallite size [17, 19–24] and surface phonon modes [18, 19, 25, 26]. However, in some cases also the strain [27, 28] and disorder [29] effects are taken into account.

In a crystallite of finite size, typically of the order of  $10 \text{ nm}$ , a phonon can no longer be described by a planar wave, but as a wave packet whose spatial dimensions are comparable to the crystallite size [17]. This introduces a spread or uncertainty in wave vector value  $q$  which increases when the grain size decreases because the wave packet becomes more localized in space. According to the phonon confinement model [17, 21], the first-order Raman spectrum  $I(\omega)$  in a semiconductor microcrystallite is given by

$$I(\omega) = \sum_j A_j \int \frac{d^3q |C(0, \vec{q})|^2}{[\omega - \omega_j(\vec{q})]^2 + (\Gamma_0/2)^2} \quad (3)$$

where  $j$  is the number of phonon bands,  $A_j$  is a coefficient,  $\omega_j(\vec{q})$  is the phonon dispersion curve,  $\Gamma_0$  is the line width (FWHM in the bulk crystal),  $C(0, \vec{q})$  is the Fourier coefficient of the phonon confinement function  $W(\vec{r}, L)$ ,  $L$  being the nanocrystal diameter and  $\vec{r}$  – radius-vector. The integration in Eq. (3) is performed over the entire Brillouin zone. The choice of the appropriate confinement function, which depends on the nanocrystal geometry, has been optimized as [21]

$$W(\vec{r}, L) = \exp(-8\pi^2 r^2 / L^2), \quad (4)$$

with the corresponding Fourier coefficient for rod-shaped crystallites

$$|C(0, q_1, q_2)|^2 \cong \exp(-q_1^2 L_1^2 / 16\pi^2) \times \exp(-q_2^2 L_2^2 / 16\pi^2) \times \left| 1 - \operatorname{erf}\left(\frac{iq_2 L_2}{\sqrt{32\pi}}\right) \right| \quad (5)$$

where  $q_1, q_2, L_1, L_2$  are the wave vectors and the nanocrystal size parameters across and along the nanocolumn, respectively, and the error function is given by

$$\operatorname{erf}x = \frac{2}{\sqrt{\pi}} \int_0^x \exp(-t^2) dt \quad (6)$$

The average phonon dispersion is usually taken in a simplified way as [19]

$$\omega_j(\vec{q}) = \omega_{j0} - \Delta\omega_j \sin^2(q/4), \quad (7)$$

where  $\omega_{j0}$  and  $\Delta\omega_j$  are the zone-centre phonon frequency and the maximal phonon dispersion of the  $j$ -th phonon branch, respectively. As far as we know, there are no explicit experimental data regarding

the dispersion of phonon branches in SbSI across the Brillouin zone. Therefore, in our calculations we have varied  $\Delta\omega$  as an adjustment parameter. The results of the calculated phonon confinement-related effect on the shape of the Raman bands at 107 and 139  $\text{cm}^{-1}$  with the nanocrystal size decrease are illustrated by Fig. 5. The values of FWHM for the bulk crystals  $\Gamma_0$  (7 and 8.5  $\text{cm}^{-1}$  for the two discussed bands, respectively) were taken from [14].

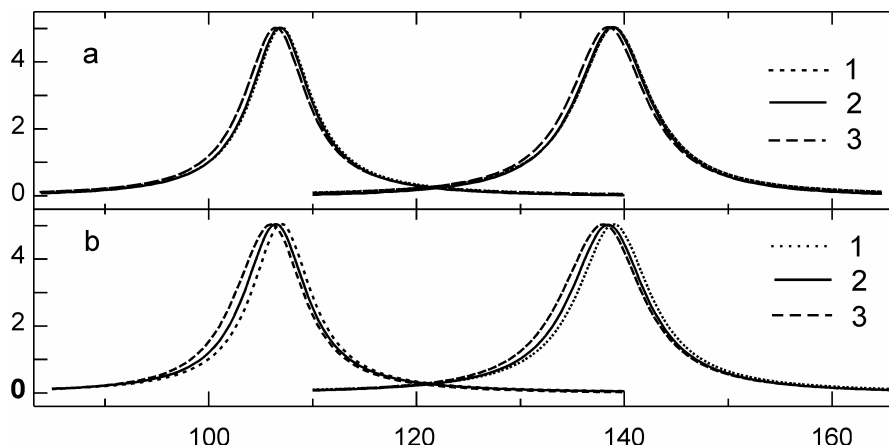


Fig. 5. Calculation of confinement-related selection rules relaxation effect upon the Raman spectra of SbSI nanocrystals. (a) calculated Raman lineshape of the bands at 107 and 139  $\text{cm}^{-1}$  for the average size of nanocrystals  $20 \times 20 \times 100 \text{ nm}^3$  (1),  $5 \times 5 \times 20 \text{ nm}^3$  (2),  $2 \times 2 \times 10 \text{ nm}^3$  (3) with the phonon branch dispersion 10  $\text{cm}^{-1}$  for both bands; (b) calculated Raman lineshape of the same bands for the average size of nanocrystals  $2 \times 2 \times 10 \text{ nm}^3$  with the phonon branch dispersion 10  $\text{cm}^{-1}$  (2) and 20  $\text{cm}^{-1}$  (3) for both bands compared with the lineshape for the bulk crystal (1).

The performed calculations have shown that the confinement-related factor would not change the Raman spectra of SbSI rod-shaped nanocrystals with the size down to  $20 \times 20 \times 100 \text{ nm}^3$ . As can be seen from the figure, the confinement-related effects begin to be revealed in the Raman spectra of SbSI nanocrystals only in case the size parameters being reduced down to 5–10 nm when the line shift and broadening can be traced (Fig. 5, a), though even then they are hardly above the instrumental errors. Note that the phonon dispersion variation in the reasonable range (up to 20  $\text{cm}^{-1}$ ) also gives rise to some noticeable changes in the spectra only for the crystallites with the size below 10 nm (Fig. 5, b). Since such values are far below those estimated from the TEM images for SbSI nanocrystals in our case, it is quite reasonable to conclude that the confinement-related wavevector selection rules relaxation cannot be the main reason, responsible for the observed size-dependent behaviour of SbSI Raman spectra, and therefore another factor, namely scattering by surface phonon modes, should be invoked for explanation.

The theory of surface phonon modes, arising in crystals due to the finiteness of their size, is well elaborated, especially for ferroelectrics [30]. Due to the size decrease in nanocrystals the surface-to-bulk contribution ratio into the Raman spectrum is much higher than in bulk crystals. Therefore, one might expect Raman observation of so-called Fröhlich surface phonon modes [25] whose frequencies are usually somewhat below those for the corresponding longitudinal bulk phonons while the surface phonons bands are considerably broader. Since in our case the frequencies of the discussed phonon modes are only slightly above 100  $\text{cm}^{-1}$ , the shift of the band frequency due to the increase of the surface phonon contribution could hardly be detected. However, the broadening of the Raman lines by a factor of about 2 in the course of milling is quite consistent with the increase of the surface-to-bulk ratio.

#### 4. Conclusions

Nanometric crystals of SbSI were obtained by milling, their rod-like shape and average size being determined from TEM measurements. As follows from the X-ray diffraction studies, the decrease

of SbSI grain size is much slowed down after the first hour of milling when the average transverse size of the crystallites of about 100 nm is achieved. This fact is discussed in view of the chain-like crystalline structure of SbSI and the difference in the nature of the interchain and intrachain forces. In the Raman spectra of SbSI nanocrystals with the average rod thickness down to  $\sim 70$  nm the bands at 107 and  $139\text{ cm}^{-1}$  are observed, the possible factors determining their broadening when the size decreases are considered: phonon confinement-related selection rules relaxation and scattering by surface phonons. The performed calculations show the confinement-related factor to be negligible in comparison with the surface phonon contribution.

### Acknowledgement

The authors are grateful to I. Makauz for the support in the technology of crystals. This joint international research was promoted by the Ukrainian-Hungarian bilateral co-operation grant UK-2/02.

### References

- [1] T. Kanata, T. Yoshikawa, K. Kubota, *Solid State Commun.* **62**, 765 (1987).
- [2] K. Ishikawa, K. Yoshikawa, N. Okada, *Phys. Rev. B* **37**, 5852 (1988).
- [3] W. L. Zhong, Y. G. Wang, P. L. Zhang, B. D. Qu, *Phys. Rev. B* **50**, 698 (1994).
- [4] D.-L. Yao, Y.-Z. Wu, Z.-Y. Li, *phys. stat. sol. B*, **231**, 3 (2002).
- [5] Y. Xu, F. Del Monte, J. D. Mackenzie, K. Namjoshi, P. Muggli, C. Joshi, *Ferroelectrics* **230**, 11 (1999).
- [6] V. M. Rubish, *J. Optoelectron. Adv. Mater.* **3**(4), 941 (2001).
- [7] L. M. Belyayev, L. A. Lyakovitskaya, G. V. Netesov, *Neorganicheskie Materialy* **1**, 2178 (1965).
- [8] H. Bakker, L. M. Di, D. M. R. Lo Cascio, *Solid State Phenomena* **23-24**, 253 (1992).
- [9] A. Guinier. *Théorie et technique de la radiocristallographie*. 2<sup>e</sup> edition. Dunod, Paris (1956).
- [10] *Struktura i Fizicheskie Svoistva Tverdogo Tela*, L. S. Palatnik (Ed.), Vyscha Shkola, Kiev (1983).
- [11] Y. Yomada, H. Chihara, *J. Phys. Soc. Jap.* **21**, 327 (1966).
- [12] M. Balkanski, M. K. Teng, S. M. Shapiro, M. K. Ziolkiewicz, *phys. stat. sol. B* **44**, 355 (1971).
- [13] D. K. Agrawal, C. H. Perry, *Phys. Rev. B*, **4**, 1893 (1971).
- [14] E. Furman, O. Brafman, J. Makovsky, *Phys. Rev. B* **8**, 2341 (1973).
- [15] H. Richter, Z. P. Wang, L. Ley, *Solid State Commun.* **39**, 625 (1981).
- [16] S. Hayashi, K. Yamamoto, *Superlattices and Microstructures* **2**, 581 (1986).
- [17] P. M. Fauchet, I. H. Campbell, *Critical Reviews in Solid State and Materials Sciences* **14**, S79 (1988).
- [18] A. Mlayah, A. M. Brugman, R. Carles, J. B. Renucci, M. Ya. Valakh, A. V. Pogorelov, *Solid State Commun.* **90**, 567 (1994).
- [19] A. Roy, A. K. Sood, *Phys. Rev. B*, **53**, 12127 (1996).
- [20] A. Ingale, K. C. Rustagi, *Phys. Rev. B*, **58**, 7197 (1998).
- [21] I. H. Campbell, P. M. Fauchet, *Sol. St. Commun.* **58**, 739 (1986).
- [22] C. Trallero-Giner, A. Debernardi, M. Cardona, E. Menendez-Proupin, A. I. Ekimov, *Phys. Rev. B* **57**, 4664 (1998).
- [23] A. A. Sirenko, V. I. Belitsky, T. Ruf, M. Cardona, A. I. Ekimov, C. Trallero-Giner, *Phys. Rev. B* **58**, 2077 (1998).
- [24] X.-Q. Li, Y. Arakawa, *Solid State Commun.* **109**, 351 (1999).
- [25] S. Hayashi, R. Ruppini, *J. Phys. C: Solid State Phys.* **18**, 2583 (1985).
- [26] Y. N. Hwang, S. H. Park, D. Kim, *Phys. Rev. B* **59**, 7285 (1999).
- [27] G. Scamarcio, M. Lugara, D. Manno, *Phys. Rev. B* **45**, 13792 (1992).
- [28] Y. N. Hwang, S. Shin, H. L. Park, S. H. Park, U. Kim, H. S. Jeong, E. J. Shin, D. Kim, *Phys. Rev. B* **54**, 15120 (1996).
- [29] M. I. Vasilevskiy, A. G. Rolo, M. J. M. Gomes, O. V. Vikhoroza, C. Ricolleau, *J. Phys.: Condens. Matter.* **13**, 3491 (2001).
- [30] M. G. Cottam, D. R. Tilley, B. Žekš, *J. Phys. C: Solid State Phys.* **17**, 1793 (1984).